



Orbital motion and quasi-periodic oscillations with periastron and Lense–Thirring precession of slowly rotating Einstein–Æther black hole

Yong Liu^{1,a}, G. Mustafa^{2,4,b}, S. K. Maurya^{3,c} , Faisal Javed^{2,d}

¹ School of Mathematics and Statistics, Changshu Institute of Technology, Suzhou 215500, People's Republic of China

² Department of Physics, Zhejiang Normal University, Jinhua 321004, People's Republic of China

³ Department of Mathematical and Physical Sciences, College of Arts and Sciences, University of Nizwa, P.O. Box 33, Nizwa 616, Sultanate of Oman

⁴ New Uzbekistan University, Mustaqillik Ave. 54, Tashkent 100007, Uzbekistan

Received: 8 April 2023 / Accepted: 8 June 2023
© The Author(s) 2023

Abstract We study the orbital and oscillatory motion of test particles moving around slowly rotating first and second kinds of Einstein–Æther black holes. In relation to the black hole parameters, we find analytical solutions for the radial profiles of specific energy and specific angular momentum of the equatorial stable circular orbits. The properties of the co-rotating as well as contra-rotating innermost stable circular orbits are analyzed. We examine the radial profiles of the frequencies of latitudinal and radial harmonic oscillations as a function of the black hole mass and dimensionless coupling constants of the theory. The key features of quasi-periodic oscillations of test particles near the stable circular orbits in an equatorial plane of the black hole are discussed. We investigate the positions of resonant radii for high-frequency quasi-periodic oscillations models, namely epicyclic resonance and its variants, relativistic precession and its variants, tidal disruption, as well as warped disc models, considered in the background of slowly rotating first and second kinds of slowly rotating Einstein–Æther black holes. Furthermore, Periastron and Lense–Thirring precessions have been discussed. We demonstrate that the dimensionless coupling parameters of the theory have a strong influence on particle motion around Einstein–Æther black holes.

1 Introduction

General relativity (GR) is a theory of gravitation that was proposed by Albert Einstein in 1915 [1]. GR has served as the most successful theory of gravitation to explain and understand various mysteries of the astrophysical as well as the cosmological realm. One needs to modify GR with the aim to avoid the fundamental issues of the theory. These issues are related to the existence of a singularity at the origin of most vacuum solutions of Einstein's equation, the inconsistency of GR with the quantum field, etc. On the other hand, the modifications to GR and the alternative theories of gravity may be considered a step forward in developing a unified theory of the interactions. One of the key principles of both modern physics and Einstein's GR is Lorentz's invariance. Another piece of evidence for the significance of the Lorentz invariance is considered to be the capability of GR to describe all observed gravitational events and its natural mathematical elegance [2]. Lorentz invariance, on the other hand, may not be a precise symmetry at all energies [3]. Any successful description must fail at some point, indicating the appearance of new physical degrees of freedom beyond that point. Lorentz invariance also causes divergences in quantum field theory, which can be rectified by a short cutoff distance that breaks it [4].

Attempts to solve problems in modern physics that are outside the scope of local Lorentz symmetry are fascinating [5]. Einstein Æther (EÆ) theory is considered a covariant-based modified theory of gravitation, which violates the Lorentz symmetry locally. Its action consists of the Einstein–Hilbert term coupled with a dynamical, unit timelike vector field, v^α , named as Æther. The rotational symmetry in a preferred

^a e-mail: liuyong@cslg.edu.cn

^b e-mail: gmustafa3828@gmail.com (corresponding author)

^c e-mail: sunil@unizwa.edu.om (corresponding author)

^d e-mail: faisaljaved.math@gmail.com

frame is retained, while local boost invariance v^α is broken [6]. Thus \mathcal{AE} ther is a type of locally favored state of rest at each location in spacetime as a result of unexplained physics. The Lorentz symmetry breaking in the gravity sector can be effectively described by the \mathcal{AE} theory, which has been extensively used to figure out the quantitative restrictions on Lorentz-violating gravity. In contrast to general relativity, the presence of \mathcal{AE} ther field in \mathcal{AE} ther theory establishes a preferred timelike direction that violates Lorentzian symmetry [7].

The motion of charged or neutral particles around black holes (BHs) is one of the most fascinating issues in BH astrophysics. It is essential for determining spacetime's geometric structure. The study of the general relativistic motion of particles and the electromagnetic fields near to BHs are now motivated by new observational and theoretical evidence for BHs. Astronomical investigations over the past ten years have shown the existence of supermassive BHs as well as stellar mass in galactic centers and X-ray binary systems. It has long been known that stellar-mass BH binaries exhibit quasi-periodic oscillations in the X-ray flux light curves, and this phenomenon is regarded as one of the most effective tests of strong gravity models. These fluctuations are closely proximity to the BH, and expressed frequencies scale inversely with the BH mass. According to the current developments, we can accurately measure the frequencies of QPOs, at center and its surroundings. It is possible to classify quasi-periodic oscillations (QPOs) into subclasses based on their measured frequencies less than 0.5 kHz. Most of these are high-frequencies (HF) and low-frequencies (LF) QPOs with frequencies up to 500 Hz and up to 30 Hz, respectively. The twin peaks with a frequency ratio 3:2 close to are often steady and detectable indicators of HF QPO oscillations in BH microquasars [8]. The QPOs around BHs (non-rotating:rotating) and wormholes have been discussed in several papers [9–13].

It is quite intriguing to investigate the properties of BHs in the presence of an \mathcal{AE} ther field. In the \mathcal{AE} theory, two spherically symmetric and static BH solutions have recently been presented, with the two combinations in coupling constants [14, 15]. Additional spherically symmetric BH solutions in the background of a class of coupling constants have been examined via numerical computing [7], and their analytical description in polynomial form has been used in the exploration of quasi-normal modes in \mathcal{AE} theory [16, 17]. The neutral particle dynamics surrounding non-spinning \mathcal{AE} BHs have been investigated in [18], while the shadow and deflection angles for slowly rotating \mathcal{AE} BHs have been probed in [19].

A productive method for exploring the phenomena surrounding BHs involves studying QPOs observed in microquasars. Precise frequency measurements of QPOs can provide valuable insight into the central object. Various types of

QPOs have been categorized based on their frequency, which can range from just a few millihertz to 0.50 kHz. The concept of QPOs are characterized by low and high-frequency ranges. BH microquasars typically exhibit high-frequency QPOs with dual peaks, whose frequency ratio closely corresponds to the ratio [20]. Multiple studies have investigated high-frequency QPOs of neutral [21], spinning [22] and charged test particles [23, 24] in the vicinity of rotating and non-rotating BHs. Recently, alternative rotating spacetimes have been explored using hot-spot data surrounding Sgr A* [25].

In the present paper, we study the orbital and epicyclic motion of neutral test particles in the background of the first and second kinds of slowly rotating \mathcal{AE} BHs. We obtain the analytical expressions for specific energy and specific angular momentum of equatorial circular orbits and investigate the properties of both co-rotating as well as counter-rotating ISCOs. We explore the perturbed motion of stable circular orbits located in an equatorial plane and examine the radial profiles of the radial, vertical, and axial frequencies in dependence on the BH mass and parameters of the BHs. Furthermore, we examine the position of resonant radii of HF QPOs models, i.e., epicyclic resonance (ER) and its variants, relativistic precession (RP) and its variants, tidal disruption (TD), as well as warped disc (WD) models. The Periastron and Lense–Thirring Precession have also been discussed.

Throughout the calculations, we consider the geometric units $G = c = 1$, and the spacetime signature $(-, +, +, +)$. Greek indices are taken to run from 0 to 3. However, for expressions having astrophysical relevance we use the physical constants explicitly.

2 Slowly rotating Einstein– \mathcal{AE} ther black hole

The slowly rotating \mathcal{AE} BH solution is an asymptotically flat solution of the field equations in \mathcal{AE} theory. The line element describing the geometry of this BH with mass M , and electric charge Q can be given as [26, 27]

$$ds^2 = -f(r)dt^2 + \frac{1}{f(r)}dr^2 + r^2(d\theta^2 + \sin^2\theta d\phi^2) - \frac{4a}{r}M\sin^2\theta dt d\phi + O(\epsilon^2). \quad (1)$$

Two types of exact solutions exist for slowly rotating \mathcal{AE} BHs. The first solution (termed as the first kind of slowly rotating \mathcal{AE} BH) corresponds to the special choice of coupling constant, i.e., $c_{14} = 0$, $c_{123} \neq 0$, where $c_{123} = c_1 + c_2 + c_3$, $c_{14} = c_1 + c_4$, and the metric function $f(r)$ for this case can be written as

$$f(r) = 1 - \frac{2M}{r} + \frac{Q}{r^2} - \frac{27M^4c_{13}}{16r^4(1 - c_{13})}, \quad (2)$$

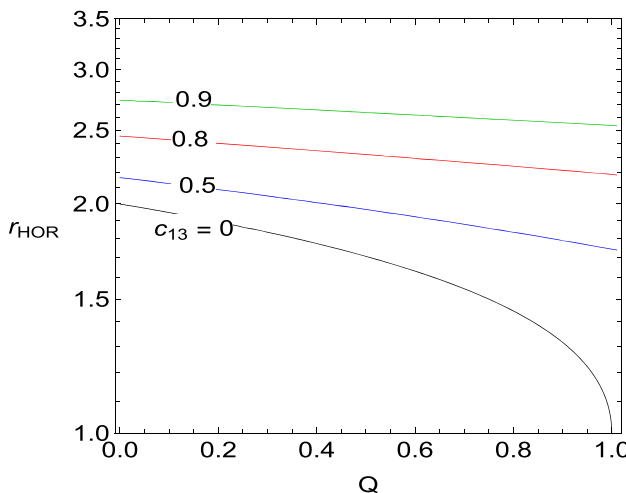


Fig. 1 Position of the horizon of the first kind of slowly rotating E&E BH as a function of charge Q , for different values of coupling parameter c_{13}

where $c_{13} = c_1 + c_3$. For $c_{13} = Q = 0$, and $a = c_{13} = 0$, the first kind of slowly rotating E&E BH reduces to the classical slowly rotating Kerr BH, and RN BH, respectively, while $a = c_{13} = Q = 0$, leads to the Schwarzschild BH. The outer horizon for the first kind of slowly rotating E&E BH can be found by solving $f(r) = 0$. The second solution (termed as the second kind of slowly rotating E&E BH) corresponds to $c_{123} = 0$, and the metric function $f(r)$ for this case can be written as

$$f(r) = 1 - \frac{2M}{r} + \frac{Q}{r^2(1 - c_{13})} + \frac{M^2(c_{14} - 2c_{13})}{2r^2(1 - c_{13})}. \quad (3)$$

For $c_{13} = c_{14} = Q = 0$, the second kind of slowly rotating E&E BH reduces to the classical slowly rotating Kerr BH. Moreover, $c_{13} = c_{14} = a = 0$, leads to the RN BH, while $c_{13} = c_{14} = a = Q = 0$, corresponds to the Schwarzschild BH. The outer horizon for the second kind of slowly rotating E&E BH is situated at

$$r_+ = M + \frac{\sqrt{(c_{14} - 2)M^2 + 2Q}}{\sqrt{2(c_{13} - 1)}}. \quad (4)$$

There are the number of observational and theoretical bounds on coupling constants c_i . In the present work, we impose the following constraints [28]

$$0 \leq c_{14} < 2, \quad 0 \leq c_{13} < 1, \quad 3c_2 + c_{13} + 2 > 0. \quad (5)$$

The positions of horizons for the first and second kinds of slowly rotating E&E BHs have shown in Figs. 1 and 2, respectively. Note that the horizons of slowly rotating E&E BHs do not depend on the rotation parameter a of BH. The horizon of the first kind of BH decreases with the increase

of charge Q , while it increases as the coupling parameter c_{13} increases. However, for the second kind of BH, the radii of horizons decrease as the coupling parameter c_{14} increases. The E&E BHs have a greater radius of the horizon as compared to RN BHs.

3 Circular orbits around E&E BH

The motion of a neutral particle can be described by the Hamiltonian given by

$$H = \frac{1}{2}g^{\alpha\beta}p_\alpha p_\beta + \frac{1}{2}m^2, \quad (6)$$

where m is the mass of the particle, $p^\alpha = mu^\alpha$ represents the four-momentum, $u^\alpha = dx^\alpha/d\tau$ denotes the four-velocity, and τ is the proper time of the test particle. The Hamilton equations of motion can be written as

$$\frac{dx^\alpha}{d\xi} \equiv mu^\alpha = \frac{\partial H}{\partial p_\alpha}, \quad \frac{dp_\alpha}{d\xi} = -\frac{\partial H}{\partial x^\alpha}, \quad (7)$$

where $\xi = \tau/m$ is the affine parameter. Due to the symmetries of the BH geometry, there exist two constants of motion, namely specific energy E and specific angular momentum L , given by

$$\frac{p_t}{m} = g_{tt}u^t + g_{t\phi}u^\phi = -\mathcal{E}, \quad (8)$$

$$\frac{p_\phi}{m} = g_{\phi\phi}u^\phi + g_{t\phi}u^t = \mathcal{L}, \quad (9)$$

where $\mathcal{E} = E/m$, $\mathcal{L} = L/m$ and the equations of motion in an equatorial plane can be written in the form [29, 30]

$$\frac{dt}{d\lambda} = \frac{\mathcal{E}r^4 - 2ar\mathcal{L}}{4a^2 + r^4f(r)}, \quad (10)$$

$$\frac{dr}{d\lambda} = \pm\sqrt{R(r)}, \quad (11)$$

$$\frac{d\theta}{d\lambda} = 0, \quad (12)$$

$$\frac{d\phi}{d\lambda} = \frac{r(2a\mathcal{E} + r\mathcal{L}f(r))}{4a^2 + r^4f(r)}, \quad (13)$$

where $R(r)$ takes the form

$$R(r) = f(r) \left[1 + \frac{r(4a\mathcal{E}\mathcal{L} + r\mathcal{L}^2f(r) - \mathcal{E}^2r^3)}{4a^2 + r^4f(r)} \right]. \quad (14)$$

Using normalization condition $g_{v\sigma}u^v u^\sigma = -1$, one can write

$$V_{eff}(r, \theta) = g_{rr}\dot{r}^2 + g_{\theta\theta}\dot{\theta}^2, \quad (15)$$

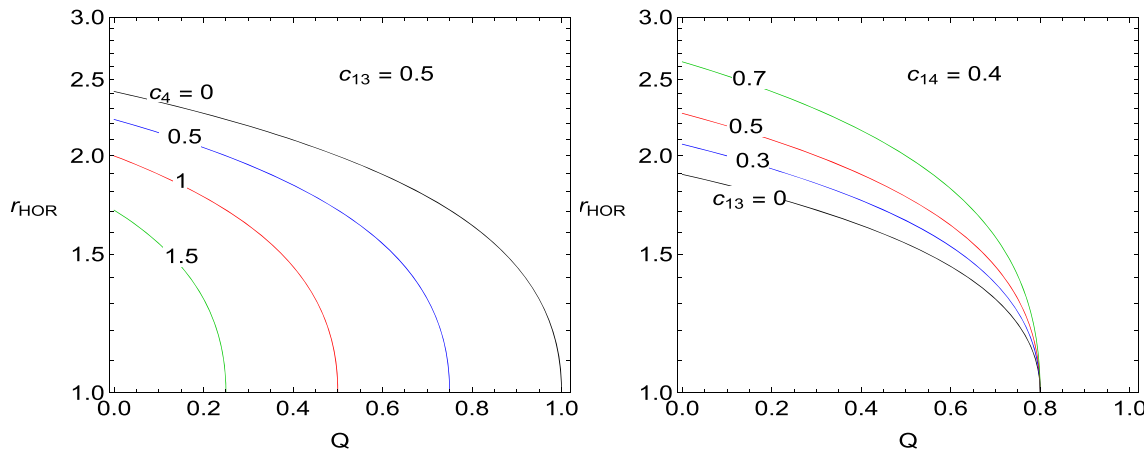


Fig. 2 Position of the horizon of second kind of slowly rotating EAE BH as a function of charge Q , for different values of parameters c_{14} (left) and c_{13} (right)

where $\dot{r} = dr/d\tau$, $\dot{\theta} = d\theta/d\tau$, and V_{eff} denotes the effective potential given by a relation

$$V_{eff}(r, \theta) = \frac{\mathcal{E}^2 g_{\phi\phi} + 2\mathcal{E}\mathcal{L}g_{t\phi} + \mathcal{L}^2 g_{tt}}{g_{t\phi}^2 - g_{tt}g_{\phi\phi}} - 1. \quad (16)$$

The effective potential $V_{eff}(r, \theta)$ plays an important role to illustrate the motion of test particles. One can describe the motion of a particle with the help of $V_{eff}(r, \theta)$ without using the equations of motion. The circular orbits for equatorial plane $\theta = \pi/2$ are given by simultaneous conditions

$$V_{eff}(r) = 0, \quad \frac{dV_{eff}(r)}{dr} = 0. \quad (17)$$

In order to find the specific energy \mathcal{E} and specific angular momentum \mathcal{L} of circular orbits, we follow the formalism of forces presented in [31, 32], and the corresponding expressions for the case of slowly rotating EAE BHs are given by the relations

$$\mathcal{E}_{(I)} = f(r) \left(1 - \frac{P_{(I)}^2(r)}{4a^2 + r^4 f(r)} \right)^{-\frac{1}{2}}, \quad (18)$$

$$\mathcal{E}_{(II)} = f(r) \left(1 - \frac{P_{(II)}^2(r)}{4a^2 + r^4 f(r)} \right)^{-\frac{1}{2}}, \quad (19)$$

$$\mathcal{L}_{(I)} = r P_{(I)}(r) \left(4a^2 + r^4 f(r) - P_{(I)}^2(r) \right)^{-\frac{1}{2}}, \quad (20)$$

$$\mathcal{L}_{(II)} = r P_{(II)}(r) \left(4a^2 + r^4 f(r) - P_{(II)}^2(r) \right)^{-\frac{1}{2}}, \quad (21)$$

where the subscripts (I) and (II) stand for the first kind and second kind of slowly rotating EAE BHs, respectively. The expressions for $P_{(I)}(r)$ and $P_{(II)}(r)$ are given by

$$P_{(I)}(r) = -3a + \sqrt{a^2 + r^2(r - Q) - \frac{27c_{13}}{16(c_{13} - 1)}}, \quad (22)$$

$$P_{(II)}(r) = -3a + \sqrt{a^2 + r^2(r + \frac{c_{14} - 2c_{13} + 2Q}{2(c_{13} - 1)})}. \quad (23)$$

The locality of stable or unstable circular orbits is consistent with the minimum or maximum of the effective potential correspondingly. In Newtonian theory, the effective potential has a minimum for any value of the angular momentum, and then it has no minimum radius of a stable circular orbit (ISCO) [33]. But this position is altered when the effective potential has a difficult form liable to the particle angular momentum and other parameters. Therefore, in GR and for the particles moving near the Schwarzschild BH, the effective potential has two extrema for any value of angular momentum. But, only for a particular value of angular momentum do the two points happen together. This point presents ISCO where is placed at $r = 3r_g$ [33–38] where r_g is the Schwarzschild radius.

The graphical behaviour of energy \mathcal{E} and angular momentum \mathcal{L} of equatorial circular orbits around the first and second kind of slowly rotating EAE BHs is depicted in Figs. 3 and 4 respectively. The energy and angular momentum of circular orbits around the first and second kinds of slowly rotating EAE BHs increases as the coupling parameter c_{13} increases, while they decrease with the increase of coupling parameter c_{14} , charge Q or rotation of BH. We compare the energy as well as the angular momentum of circular orbits around Schwarzschild, RN, Solwly rotating Kerr and slowly rotating EAE BHs, and observe that the circular orbits around slowly rotating EAE BHs have greater energy and angular momentum among all the cases.

The ISCO is located at $d^2 V_{eff}/dr^2 = 0$ and the position of co-rotating and counter-rotating ISCOs for first and second kinds of slowly rotating EAE BHs is illustrated in Figs. 5 and 6,

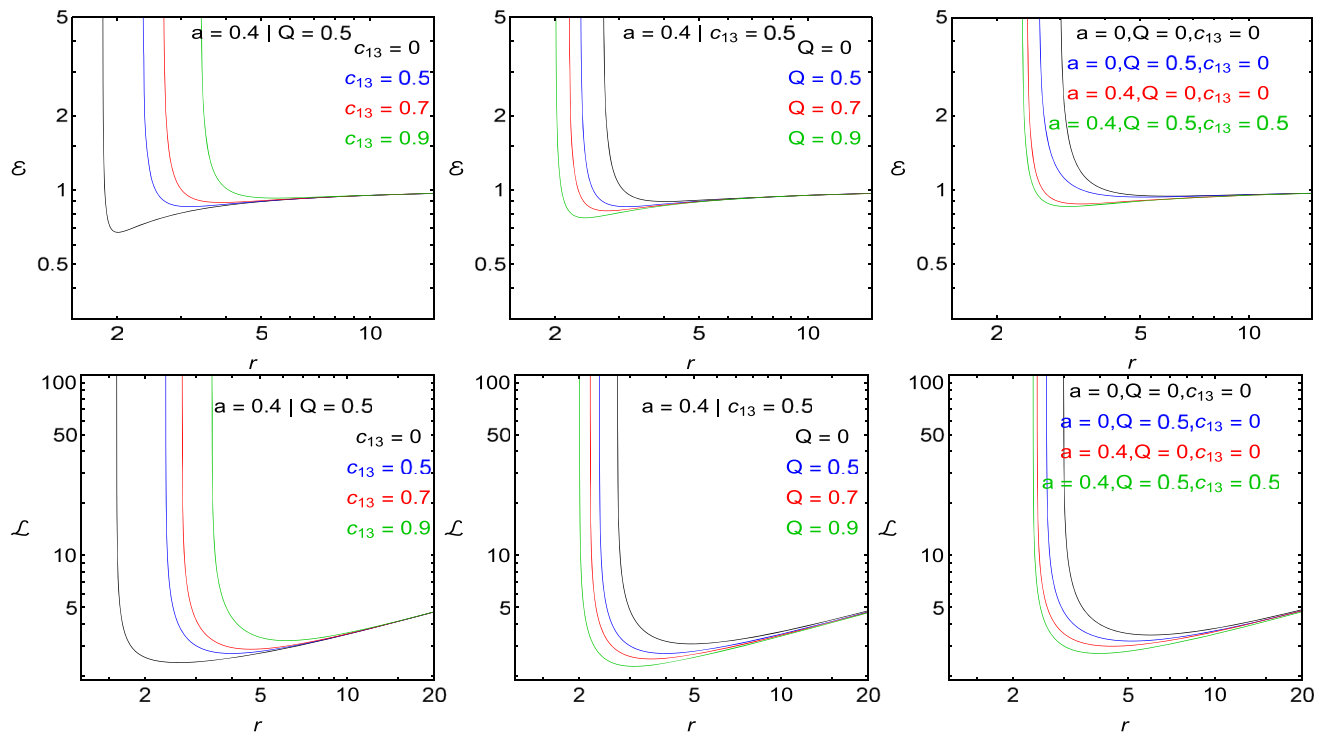


Fig. 3 Radial profiles of energy (first row) and angular momentum (second row) at the circular orbits around first kind of slowly rotating EAE BH for different values of coupling parameter c_{13} , charge Q

and rotation parameter a . The comparison between Schwarzschild, RN, slowly rotating Kerr, and slowly rotating EAE BH for energy and angular momentum has been shown in the last column

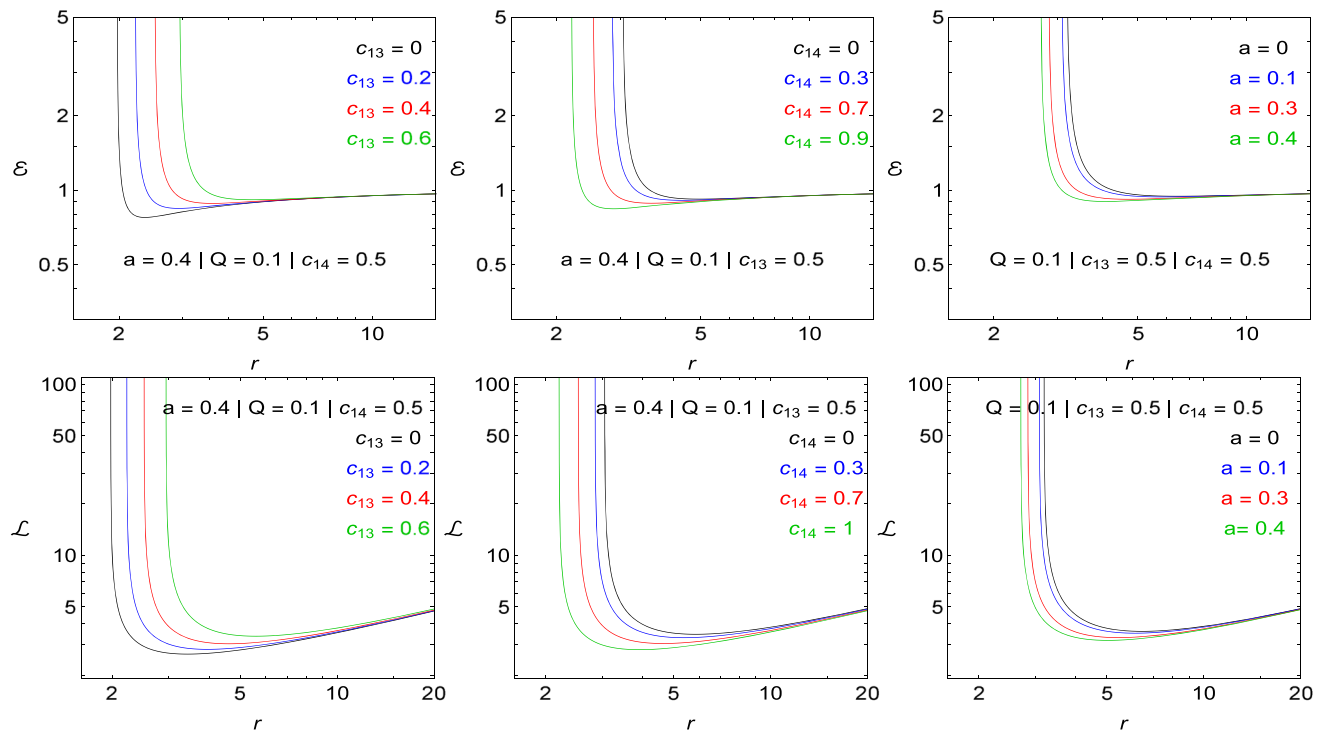


Fig. 4 Radial profiles of energy (first row) and angular momentum (second row) of second kind of slowly rotating EAE BH for different values of coupling parameters c_{13}, c_{14} and rotation parameter a

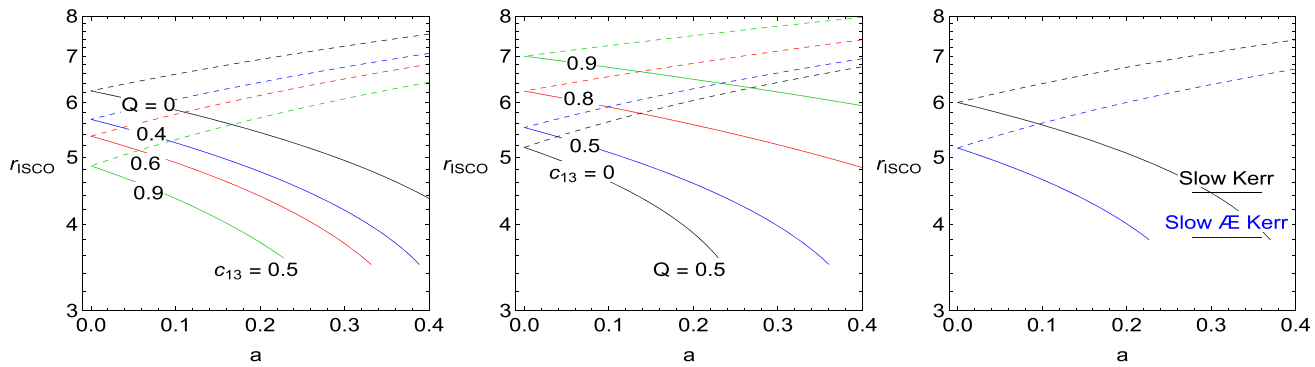


Fig. 5 Position of ISCOs of the first kind of slowly rotating EAE BH. Solid curves are for co-rotating particles, while dashed curves are plotted for counter-rotating particles. The comparison between the ISCO positions of slowly Kerr BH and the first kind of EAE BHs is shown in the last plot

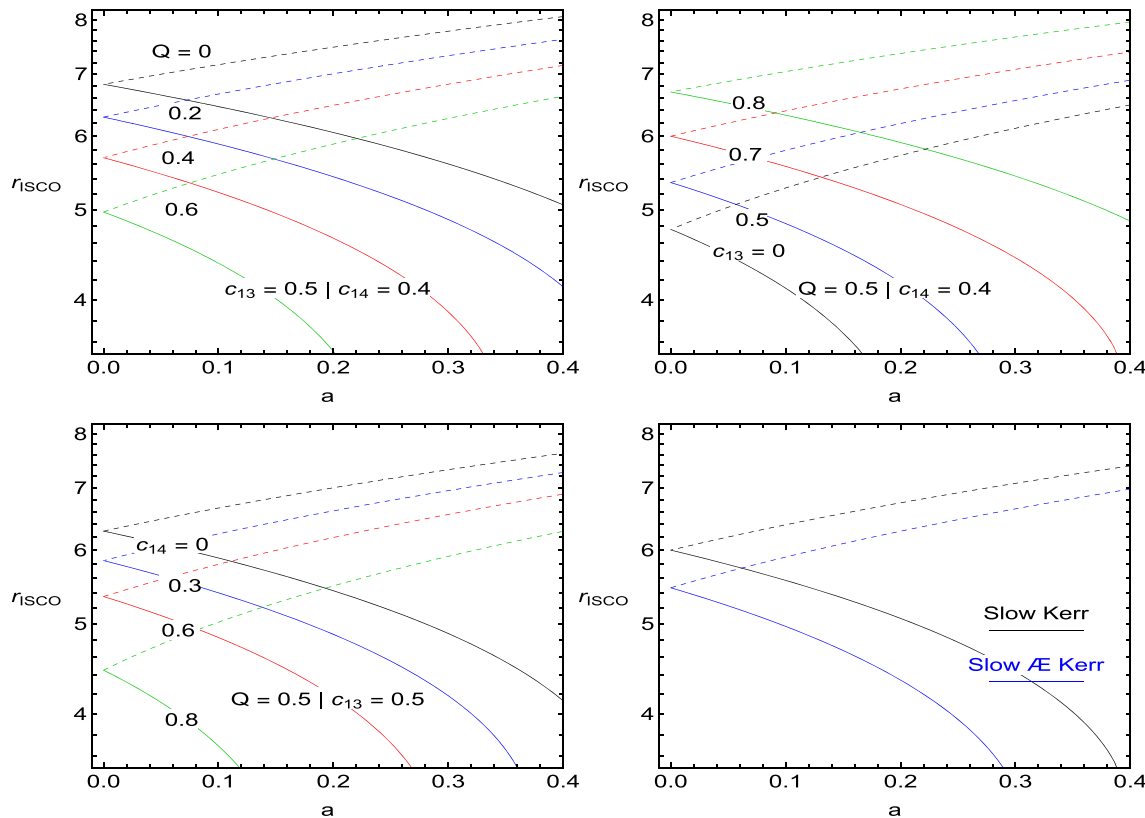


Fig. 6 Position of ISCOs of the second kind of slowly rotating EAE BH. Solid curves are for co-rotating particles, while dashed curves are plotted for counter-rotating particles. The comparison between the ISCO

positions of slowly Kerr BH and the first kind of EAE BHs is shown in the right plot of the second row

respectively. The co-rotating ISCOs shift towards the BHs, while the contra-rotating ISCOs move away from the BH with the increase of the coupling parameter c_{14} or electric charge Q . In the case of co-rotating particles, the ISCOs shift away from the BH as the coupling parameter c_{13} is increased but move towards the BH when the rotation of BH is increased. Smaller radii of ISCOs can be observed when the BHs rotate rapidly. We see that the ISCOs around the first

and second kinds of slowly rotating EAE BHs are smaller as compared to slowly rotating Kerr BH.

4 Harmonic oscillations as perturbation of circular orbits

In order to investigate the oscillatory motion of neutral particles, we perturb the equations of motion in the vicinity of

stable circular orbits. If a test particle is slightly shifted from the equilibrium position related to a stable circular orbit situated in an equatorial plane, it will undergo epicyclic motion, characterized by linear harmonic oscillations. The frequencies of harmonic oscillatory motion measured by the local observer are given by [40,41]

$$\omega_r^2 = \frac{-1}{2g_{rr}} \frac{\partial^2 V_{\text{eff}}(r, \theta)}{\partial r^2}, \quad (24)$$

$$\omega_\theta^2 = \frac{-1}{2g_{\theta\theta}} \frac{\partial^2 V_{\text{eff}}(r, \theta)}{\partial \theta^2}, \quad (25)$$

$$\omega_\phi = \frac{d\phi}{d\tau}. \quad (26)$$

The radial (ω_r), latitudinal (ω_θ), and orbital/axial (ω_ϕ) frequencies of the neutral test particle for the first and second kinds of slowly rotating EAE BH takes the form

$$\begin{aligned} \omega_{r(I)}^2 = & \frac{f(r)}{r^4 (4a^2 + f(r))^3} (16a^3(a\xi - \mathcal{E}_{(I)}\mathcal{L}_{(I)}rY) - 4a^2 \\ & \times (\sigma\nu + \mathcal{L}_{(I)}^2\psi + \mathcal{E}_{(I)}^2r^4Y) + 4\mathcal{E}_{(I)}a\mathcal{L}_{(I)}r\alpha \\ & - r^2(\sigma\mathcal{L}_{(I)}^2(9(Z-1)Z+3) + \mathcal{E}_{(I)}^2\sigma r^4\mu - 3\mathcal{L}_{(I)}^2Z^3 \\ & + \mathcal{E}_{(I)}^2r^4\eta)), \end{aligned} \quad (27)$$

$$\omega_{\theta(I)}^2 = \frac{\mathcal{L}_{(I)}f(r)(8a^2 + \mathcal{L}_{(I)}f(r)) + 4\mathcal{E}_{(I)}a^2r^3\delta}{r^4 (4a^2 + f(r))^2}, \quad (28)$$

$$\omega_{\phi(I)}^2 = \frac{(2ar^3\mathcal{E}_{(I)} + \mathcal{L}_{(I)}f(r))^2}{r^4 (4a^2 + f(r))^2}, \quad (29)$$

$$\omega_{r(II)}^2 = \frac{1}{\lambda_{12}} \left[12(c_{13}-1)\mathcal{E}_{(II)}^2\lambda_{11}^2r^2 - 2(c_{13}-1) \right. \quad (30)$$

$$\left. \times \lambda_{10}^2\mathcal{L}_{(II)}^2 + \lambda_1 + 8\lambda_2\lambda_3\lambda_4\lambda_5\lambda_6\lambda_7\lambda_8\lambda_9\lambda_{10} \right. \\ \times \mathcal{L}_{(II)}^2 \left. \right], \quad (31)$$

$$\omega_{\theta(II)}^2 = \frac{(16ra^3\mathcal{E}_{(II)}\mathcal{L}_{(II)} + \gamma r^2\mathcal{L}_{(II)}^2 + 4a^2\rho)}{(r^3(4\beta - r^2 + 2r) - 4a^2r)^2},$$

$$\omega_{\phi(II)}^2 = \frac{(\mathcal{L}_{(II)}(\beta - r(r-2)) - 2ar\mathcal{E}_{(II)})^2}{(4a^2 + r^2f(r))^2}, \quad (32)$$

where the introduced coefficients read

$$\sigma = \frac{27c_{13}}{16(c_{13}-1)r^2}, \quad \chi = (-4 + 3r),$$

$$\nu = (\mathcal{L}^2(r^2 + 9z - 6) - 12\mathcal{E}^2r^4),$$

$$\xi = (\mathcal{L}^2 - 3r^2(\sigma\mathcal{L}^2 + 2\mathcal{E}^2)),$$

$$\psi = (Q^2 + 3Qr\chi + 2r^2(2r - 3)\chi),$$

$$\eta = (Q^2 - 3Qr^2 + 2r^3), \quad \mu = (-3Q + 2r(5r - 3) + 6),$$

$$\alpha = (\sigma Y + r^2(Q^2 + 3Q(r-2)r + 2r^2(r(3r-8) + 6))),$$

$$\delta = (4a\mathcal{L}_{(I)} - \mathcal{E}_{(I)}r^3),$$

$$\beta = \frac{(2Q - 2c_{13} + c_{14})}{2(c_{13}-1)},$$

$$\begin{aligned} \gamma &= ((r-2)r - 4\beta)^2, \\ \rho &= (\mathcal{L}_{(II)}^2(2(r-2)r + \beta) - \mathcal{E}_{(II)}^2r^4), \\ \lambda_1 &= \left(-2c_{13}(r-1)^2 + c_{14} + 2(Q + (r-2)r) \right) (-32a \\ &\times (c_{13}-1)\mathcal{E}_{(II)}\mathcal{L}_{(II)}r^3(c_{13}(-4r^2 + 6r - 2) + c_{14} \\ &+ 2Q + 4r^2 - 6r)^2), \\ \lambda_2 &= (c_{13}-1)\mathcal{E}_{(II)}^2r^6(c_{13}(-4r^2 + 6r - 2) + c_{14} + 2Q \\ &+ 4r^2 - 6r)^2 - 4\mathcal{L}_{(II)}^2r^2(2c_{13}(r-1)^2 - c_{14} - 2(Q \\ &+ (r-2)r)), \\ \lambda_3 &= 16a(c_{13}-1)\mathcal{E}_{(II)}\mathcal{L}_{(II)}r(c_{13}(4r^2 - 6r + 2) - c_{14} \\ &- 2Q - 4r^2 + 6r) + (c_{13}(-4r^2 + 6r - 2) \\ &+ c_{14} + 2Q + 4r^2 - 6r)^2, \\ \lambda_4 &= (8a^2(c_{13}-1) + r^2(2c_{13}(r-1)^2 - c_{14} - 2(Q \\ &+ (r-2)r))) + 8(c_{13}-1)\mathcal{L}_{(II)}^2(r-1)r \\ &\times (c_{13}(4r^2 - 6r + 2) - c_{14} - 2Q - 4r^2 + 6r), \\ \lambda_5 &= (8a^2(c_{13}-1) + r^2(2c_{13}(r-1)^2 - c_{14} - 2(Q \\ &+ (r-2)r))) - 16(c_{13}-1)\mathcal{E}_{(II)}^2r^4 \\ &\times (c_{13}(4r^2 - 6r + 2) - c_{14} - 2Q - 4r^2 + 6r), \\ \lambda_6 &= (8a^2(c_{13}-1) + r^2(2c_{13}(r-1)^2 - c_{14} - 2(Q \\ &+ (r-2)r))) + 8a(c_{13}-1)\mathcal{E}_{(II)}\mathcal{L}_{(II)} \\ &\times r(2c_{13}(6r^2 - 6r + 1) - c_{14} - 2(Q + 6(r-1)r)), \\ \lambda_7 &= (8a^2(c_{13}-1) + r^2(2c_{13}(r-1)^2 - c_{14} - 2(Q \\ &+ (r-2)r))) - 2(c_{13}-1)\mathcal{E}_{(II)}^2r^4 \\ &\times (2c_{13}(6r^2 - 6r + 1) - c_{14} - 2(Q + 6(r-1)r)), \\ \lambda_8 &= 8a^2(c_{13}-1) + r^2(2c_{13}(r-1)^2 - c_{14} - 2(Q \\ &+ (r-2)r)), \\ \lambda_9 &= (2c_{13}(r-1)^2 - c_{14} - 2(Q + (r-2)r))(2c_{13} \\ &\times (6r^2 - 6r + 1) - c_{14} - 2(Q + 6(r-1)r)), \\ \lambda_{10} &= 8a^2(c_{13}-1) + r^2(2c_{13}(r-1)^2 - c_{14} - 2(Q \\ &+ (r-2)r)), \\ \lambda_{11} &= 8a^2(c_{13}-1) + r^2(2c_{13}(r-1)^2 - c_{14} - 2(Q \\ &+ (r-2)r)), \\ \lambda_{12} &= 2(c_{13}-1)r^2(8a^2(c_{13}-1) + r^2(2c_{13}(r-1)^2 \\ &- c_{14} - 2(Q + (r-2)r)))^3. \end{aligned}$$

and the energy $\mathcal{E}_{(I)}$, $\mathcal{E}_{(II)}$, and angular momentum $\mathcal{L}_{(I)}$, $\mathcal{L}_{(II)}$ are given by Eqs. (18)–(21), respectively. The identification of different shapes of charged particle epicyclic orbits near a stable circular orbit can be facilitated by observing the behavior of the fundamental frequencies, namely ω_r , ω_θ , and ω_ϕ , as well as their respective ratios. The Newtonian theory of gravitation predicts that all frequencies are identical, resulting in

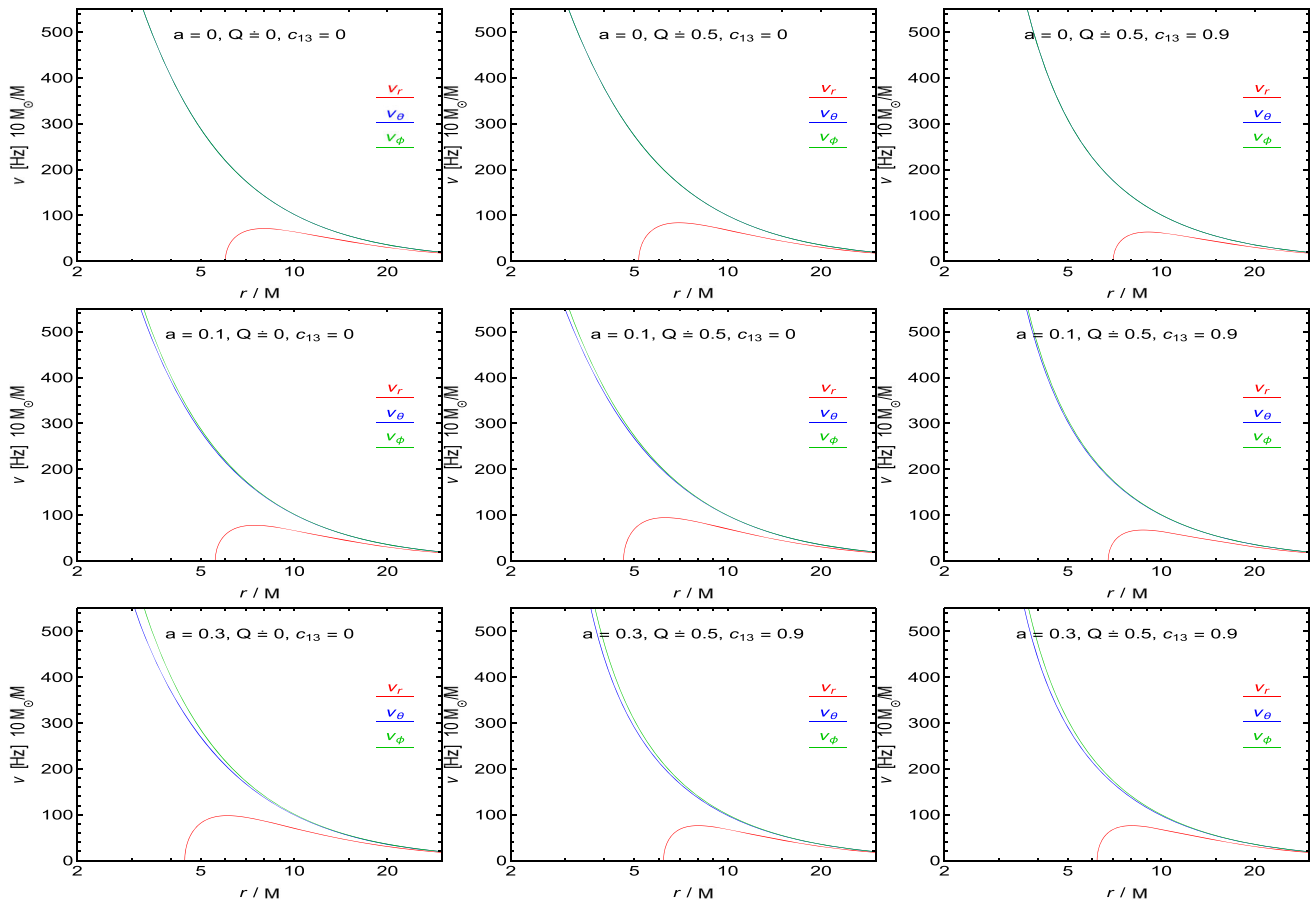


Fig. 7 Radial profiles of frequencies of small harmonic oscillations radial v_r , vertical v_θ and axial v_ϕ of a neutral particle around first kind of slowly rotating EÆ BH with BH mass $M = 10M_\odot$, measured by a static distant observer

elliptical trajectories for particles orbiting spherically symmetric bodies. However, for Schwarzschild BH, the frequencies follow the relation $\omega_r < \omega_\theta = \omega_\phi$, causing a periapsis shift and inducing relativistic precession as the radius of the orbit decreases and the strong gravity region is approached.

4.1 Frequencies measured by distant observer

The locally measured angular frequencies

$$\omega_\alpha = \frac{d\phi_\alpha}{dt}, \quad (33)$$

are related to the angular frequencies measured by the static distant observer (Ω), by the gravitational redshift transformation

$$\Omega_\alpha = \frac{d\phi_\alpha}{d\tau} = \omega_\alpha \frac{dt}{d\tau}, \quad (34)$$

where $dt/d\tau$ is the redshift coefficient. If the frequencies of small harmonic oscillations measured by the distant observer

are expressed in physical units, one needs to extend the corresponding dimensionless form by the factor c^3/GM . Thus the frequencies of the neutral particles measured by distant observers are given by [42]

$$v_j = \frac{1}{2\pi} \frac{c^3}{GM} \Omega_j [\text{Hz}], \quad (35)$$

where $j \in \{r, \theta, \phi\}$; Ω_r , Ω_θ , and Ω_ϕ denotes the dimensionless radial, latitudinal, and axial angular frequencies measured by a distant observer. The Figs. 7 and 8 display the radial profiles of frequencies v_j for small harmonic oscillations of neutral particles, as measured by an observer at a distance, around slowly-rotating EÆ BHs of both the first and second kinds, with varying spin parameter a , charge Q , and dimensionless coupling parameters c_{13} and c_{14} . As any of these parameters increase, the radial profiles shift towards the black hole. However, coupling parameter c_{13} contributes to moving the radial profiles away from the BH. The particles moving around slowly rotating Kerr BH have high frequencies as compared to moving around slowly rotating EÆ BHs.

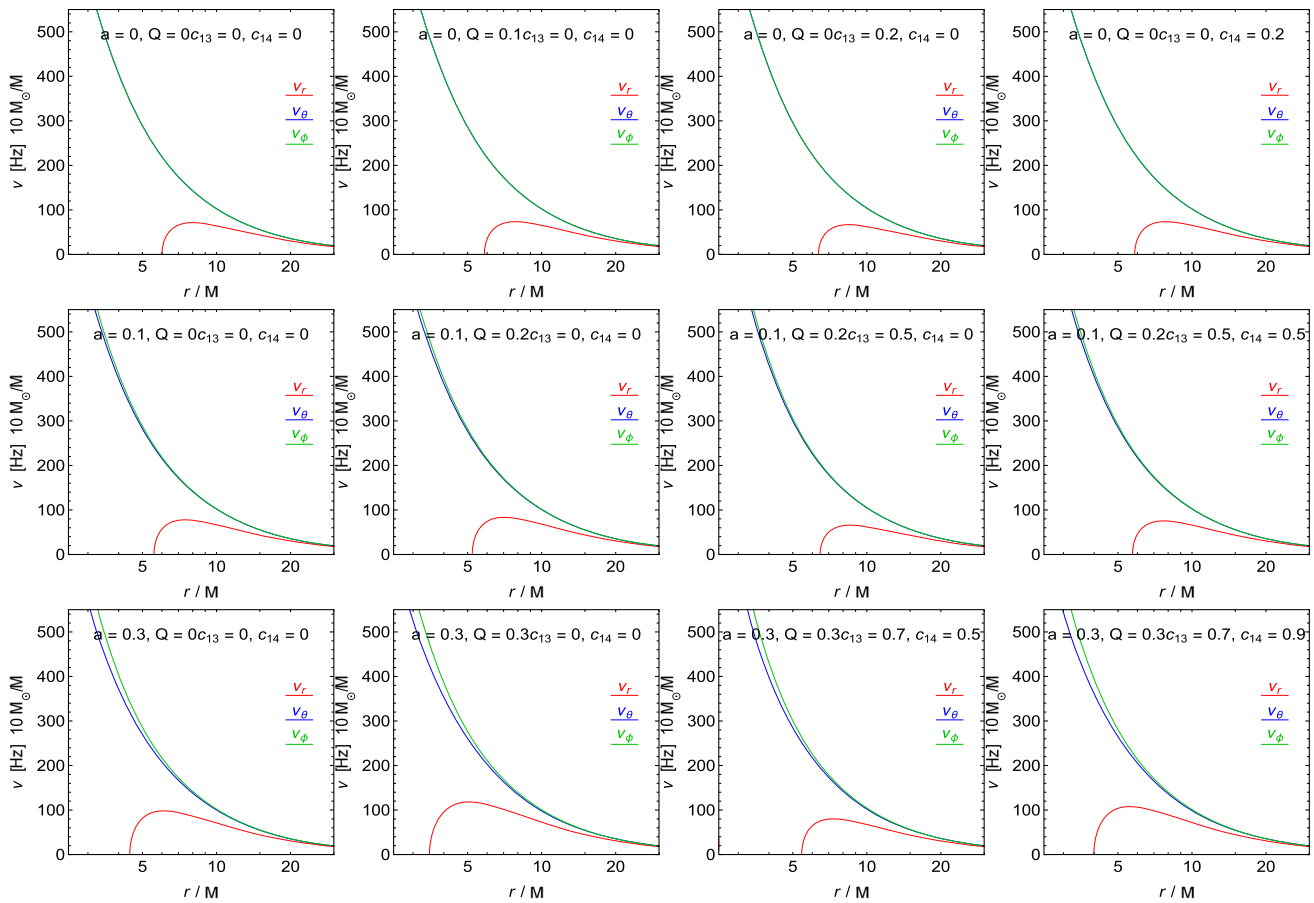


Fig. 8 Radial profiles of frequencies of small harmonic oscillations radial v_r , vertical v_θ and axial v_ϕ of a neutral particle around second kind of slowly rotating EA BH with BH mass $M = 10M_\odot$, measured by a static distant observer

5 Quasi-periodic oscillations models

The previous section's exploration of neutral particle oscillations on circular orbits has potential ramifications in astrophysics, particularly about HF QPOs detected in micro-quasars. Hot spot models hypothesize that radiating spots exist in thin accretion discs and follow nearly circular geodesic trajectories. The ER model, on the other hand, posits resonance of axisymmetric oscillation modes of accretion discs. The frequencies of these oscillations are linked to the orbital and epicyclic frequencies of circular geodesic motion. Within the ER model, which includes axisymmetric oscillatory modes at frequencies v_θ and v_r , uniform radiation is assumed to emanate from the oscillating torus (or circle). The presence of a sufficiently large irregularity on the orbiting torus, which has a frequency of v_ϕ , permits the establishment of the nodal frequency associated with this irregularity. Table 1 contains the variations of the ER model, for details, see [39]. In the standard RP model [43], the higher of the paired frequencies corresponds to the orbital (azimuthal) frequency, $v_U = v_\phi$, while the lower frequency represents the periastron precession rate, $v_L = v_\phi - v_r$. From the vari-

Table 1 The upper and lower frequencies of HF QPOs models [39]

Model	v_U	v_L
ER0	v_θ	v_r
ER1	v_θ	$v_\theta - v_r$
ER2	$v_\theta - v_r$	v_r
ER3	$v_\theta + v_r$	v_θ
ER4	$v_\theta + v_r$	$v_\theta - v_r$
ER5	v_r	$v_\theta - v_r$
RP0	v_ϕ	$v_\phi - v_r$
RP1	v_θ	$v_\phi - v_r$
RP2	v_ϕ	$v_\theta - v_r$
TD	$v_\phi + v_r$	v_ϕ
WD	$2v_\phi - v_r$	$2(v_\phi - v_r)$

ants of the RP model, we select the RP1 model introduced in [44], where $v_U = v_\theta$ and $v_L = v_\phi - v_r$, and the “total precession model” RP2 introduced in [9], where $v_U = v_\phi$ and $v_L = v_\theta - v_r$ (see Table 1). Both the RP1 and RP2 models predict frequencies v_U and v_L close to those of the RP model.

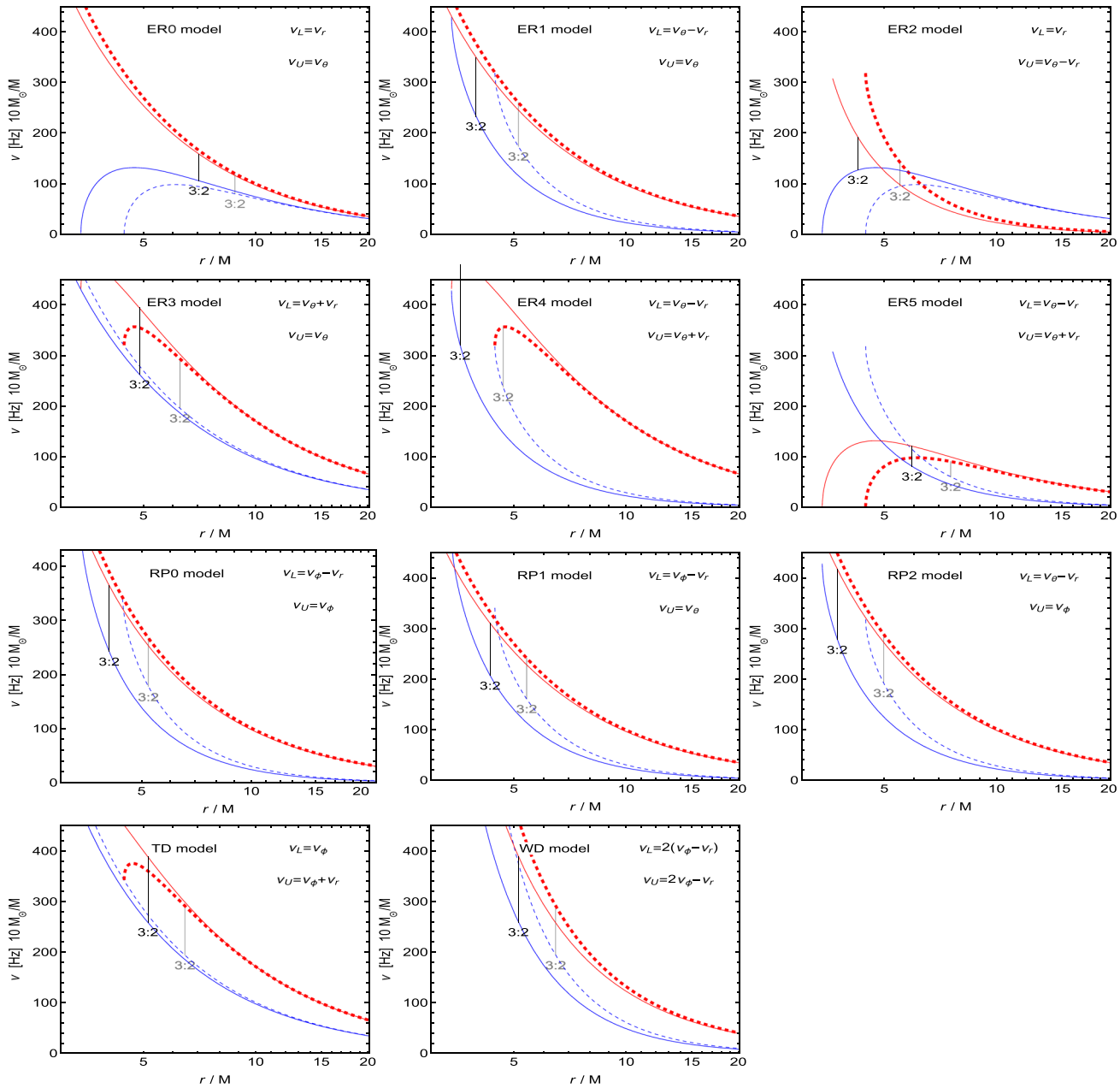


Fig. 9 Radial profiles of lower $v_L(r)$ and upper $v_U(r)$ frequencies for various HF QPOs models for first kind of slowly rotating EAE BH. Solids curves are plotted for the first kind of slowly rotating EAE BH, while dashed curves are for slowly rotating Kerr BH. Black vertical lines show

the positions of $v_U : v_L = 3 : 2$ resonance radii $r_{3:2}$ for the first kind of slowly rotating EAE BH, while gray lines are for Kerr BH. BH spin parameter $a = 0.3$ has been used in all cases

The TD model, which has $v_U = v_\phi + v_r$ and $v_L = v_\phi$, may bear some resemblance to hot spot models. This is because numerical simulations have shown that the BH tidal forces that disrupt inhomogeneities (such as asteroids) can create a ring-like structure that includes an orbiting radiating core. As for the WD oscillation model of twin HF QPOs, it assumes that there are non-axisymmetric oscillatory modes of a thin disc. In order to account for the frequencies in Table 1 of the

WD model, we must make the assumption that there are also vertical axisymmetric oscillations of the thin disc, which we will call v_θ . The radial profile of the frequencies v_U and v_L of different HF QPOs models, i.e., ER (ER0, ER1, ER2, ER3, ER4, ER5), RP (RP1, RP2, RP3), TD and WD models for both first and second kind of slowly rotating EAE BHs are illustrated in Figs. 9 and 10, respectively. We compare the frequencies in the background of HF QPOs models modified

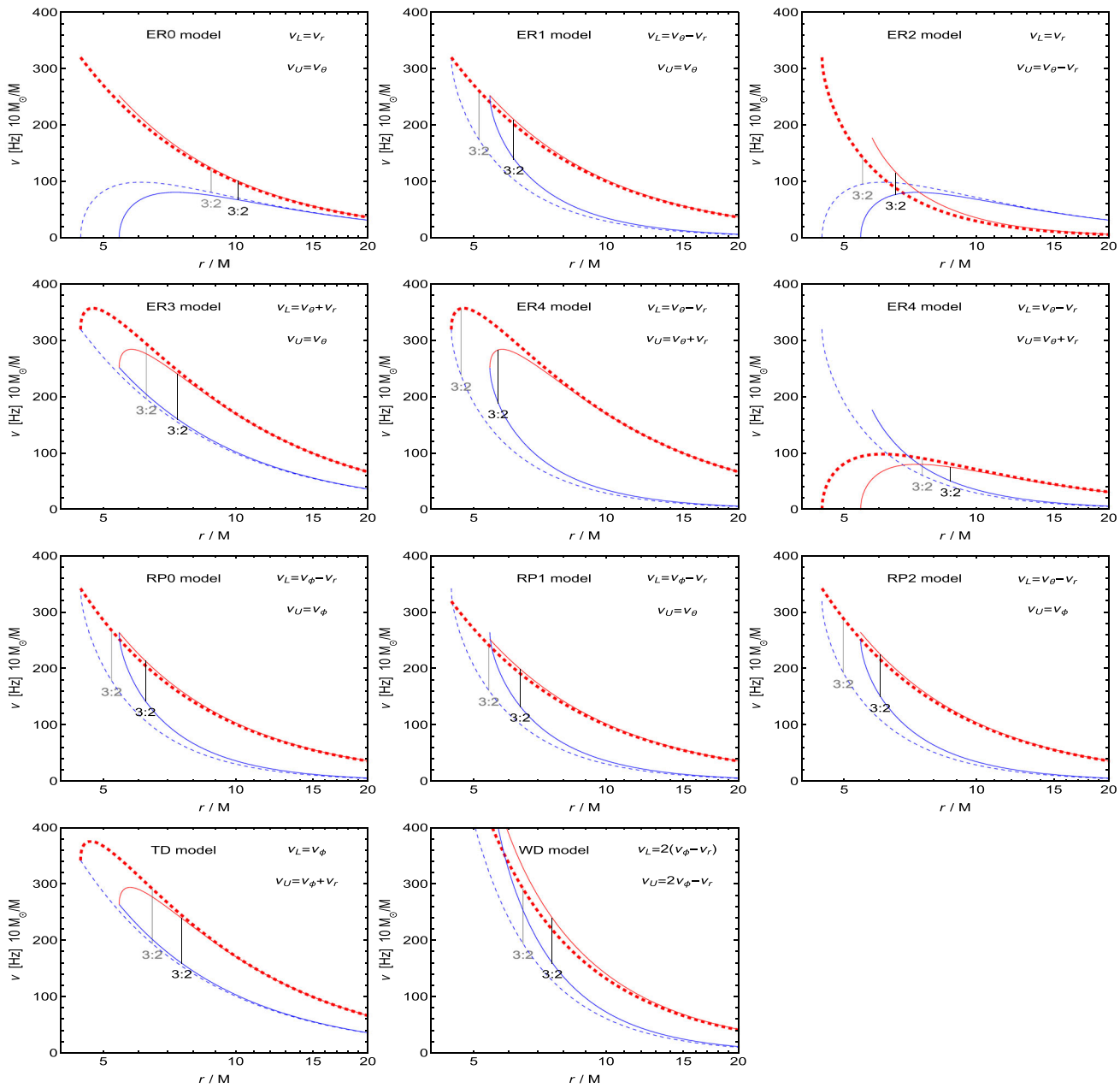


Fig. 10 Radial profiles of lower $v_L(r)$ and upper $v_U(r)$ frequencies for various HF QPOs models for the second kind of slowly rotating EAE BH. Solids curves are plotted for the second kind of slowly rotating EAE BH, while dashed curves are for slowly rotating Kerr BH. Black

vertical lines show the positions of $v_U : v_L = 3 : 2$ resonance radii $r_{3:2}$ for the second kind of slowly rotating EAE BH, while gray lines are for Kerr BH. BH spin parameter $a = 0.3$ has been used in all cases

by the particle motion around a slowly rotating EAE BHs with the motion around a slowly rotating Kerr BH and see that the particle motion deviates from the Kerr limit.

5.1 Resonant radii

The quasi-harmonic character of the motion of test particles trapped in a toroidal space around the equatorial plane of

BHs gives an interesting astrophysical application concerning the HF QPOs observed in the LMXB systems containing a neutron star or BH. The HF QPOs usually come in pairs of the upper and lower frequencies of twin peaks in the Fourier power spectra. The peaks of HFs are close to the axial frequency of the stable circular orbit denoting the inner edge of Keplerian discs orbiting BHs, thus the strong gravity effects must be relevant in explaining HF QPOs [45].

The HF QPOs usually appear in a pair of two peaks with upper ν_U and lower ν_L frequencies in the timing spectra, and the ratio of frequencies $\nu_U : \nu_L$ is close to the ratio 3:2. Observation of this effect in different non-linear systems shows the existence of the resonances between two modes of oscillations. In the case of slowly rotating E&E BHs, the upper and lower frequencies of a neutral test particle around the first and second kinds of slowly rotating E&E BHs are functions of parameters c_{13} , c_{14} resonance position r , and a BH spin a , given by

$$\nu_U = \nu_U(r, M, a, c_{13}, c_{14}), \quad \nu_L = \nu_L(r, M, a, c_{13}, c_{14}). \quad (36)$$

These frequencies ν_L and ν_U are inversely proportional to the mass M of the BH and given by Eq. (35). In order to fit the frequencies observed in HF QPOs with the BH parameters, one needs to find the resonant radii, given by a relation

$$\nu_U(r_{3:2}) : \nu_L(r_{3:2}) = 3 : 2. \quad (37)$$

In general, the resonant radii $r_{3:2}$ are given by a numerical solution of higher order polynomial in r , for given values of the BH parameters. The resonant radius solution has no

dependence on the mass of the BH as Eq. (37) is independent of the mass of the BH explicitly. The position of resonant radii $r_{3:2}$ for HF QPO models in the background of slowly rotating first and second kinds of E&E BHs have been shown in Figs. 9, and 10, respectively. We compare the case of slowly rotating Kerr BH with the slowly rotating E&E BHs and see that for all considered BH QPOs models, the position of resonant radii $r_{3:2}$ for slowly rotating E&E BHs is at smaller radii as compared to slowly rotating Kerr BH. The resonant radius $r_{3:2}$ for the ER4 HF QPOs model is closer to the BH among all considered models.

5.2 Periastron and Lense–Thirring precession

In this section, we discuss the periastron and Lense–Thirring precession frequency of a neutral test particle moving around the slowly rotating E&E BHs in the limit of a small perturbation with respect to the equatorial plane $\pi/2$. In order to calculate the Periastron precession, we assume that the particle is slightly perturbed from its stable position which in turn results in oscillations about the stable position r_s with a radial frequency Ω_r . The periastron Ω_P frequency is defined as a difference in orbital frequency Ω_ϕ and radial frequency Ω_r , while the Lense–Thirring precession frequency Ω_{LT} is

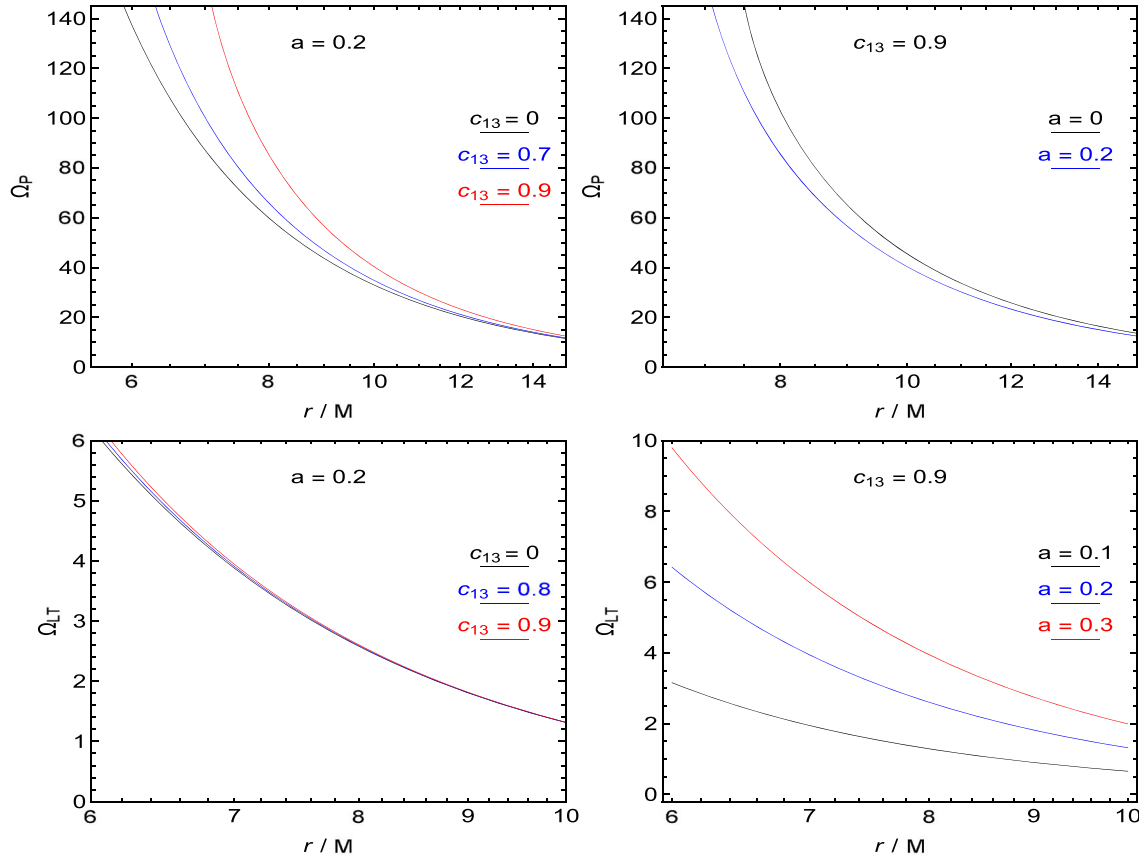


Fig. 11 Periastron and Lense–Thirring precessions for the first kind of slowly rotating E&E BH

defined as the difference in orbital frequency Ω_ϕ and latitudinal frequency Ω_θ , given by the relation

$$\Omega_P = \Omega_\phi - \Omega_r, \quad (38)$$

$$\Omega_{LT} = \Omega_\phi - \Omega_\theta, \quad (39)$$

where the orbital Ω_ϕ , radial Ω_r , and latitudinal frequencies Ω_θ are given by Eq. (34). In contrast to Newtonian gravity, when general relativistic effects are taken into consideration (close to BH), the radial and orbital frequencies are no longer equal, i.e., $\Omega_\theta \neq \Omega_\phi$. The graphical behaviour of periastron and Lense–Thirring precession frequencies for both first and second kinds of E&E BHs have been depicted in Figs. 11 and 12, respectively. Both periastron and Lense–Thirring precession frequencies increase as the coupling parameters c_{13} or c_{14} increase. However, Ω_P decreases while Ω_P increases when the BH rotates rapidly. The radial profiles of Ω_P for the case of slowly rotating Kerr BH lie above the first and second kinds of slowly rotating E&E BHs, while Ω_{LT} lies below the E&E BHs.

6 Discussion and conclusions

We have explored the orbital and oscillatory motion of neutral test particles moving around slowly rotating first and second kinds of E&E BHs and examined the influence of the BH

parameters. The positions of horizons have been investigated. The radii of the BH horizon increase with the increase of the coupling parameter c_{13} , however, it decreases as the coupling parameter c_{14} or electric charge of BH Q is increased.

Using the formalism of forces [31], we have found the analytical solutions of radial profiles of specific energy and specific angular momentum of equatorial stable circular orbits in dependence on the BH parameters and compared them with the case of slowly rotating Kerr BH. Initially, the specific energy and specific angular momentum of circular orbits grow fast as the coupling parameter c_{13} is increased, while it decreases with the increase of charge parameter Q of BH, and then becomes almost constant when the particles move away from the BH. The circular orbits close to the BH have less energy as well as angular momentum when the BH rotates rapidly or the coupling parameter c_{14} is enhanced but increases as the radial distance is increased. The circular orbits with high energy and large angular momentum can be seen around slowly rotating Kerr BH as compared to the first and second kinds of slowly rotating E&E BHs.

We have determined the positions of ISCOs for the co-rotating and contra-rotating neutral test particles orbiting slowly rotating first and second kinds of E&E BHs. We observed that the co-rotating ISCOs shift towards the BHs, while the contra-rotating ISCOs move away from the BH with the increase of the coupling parameter c_{14} or electric

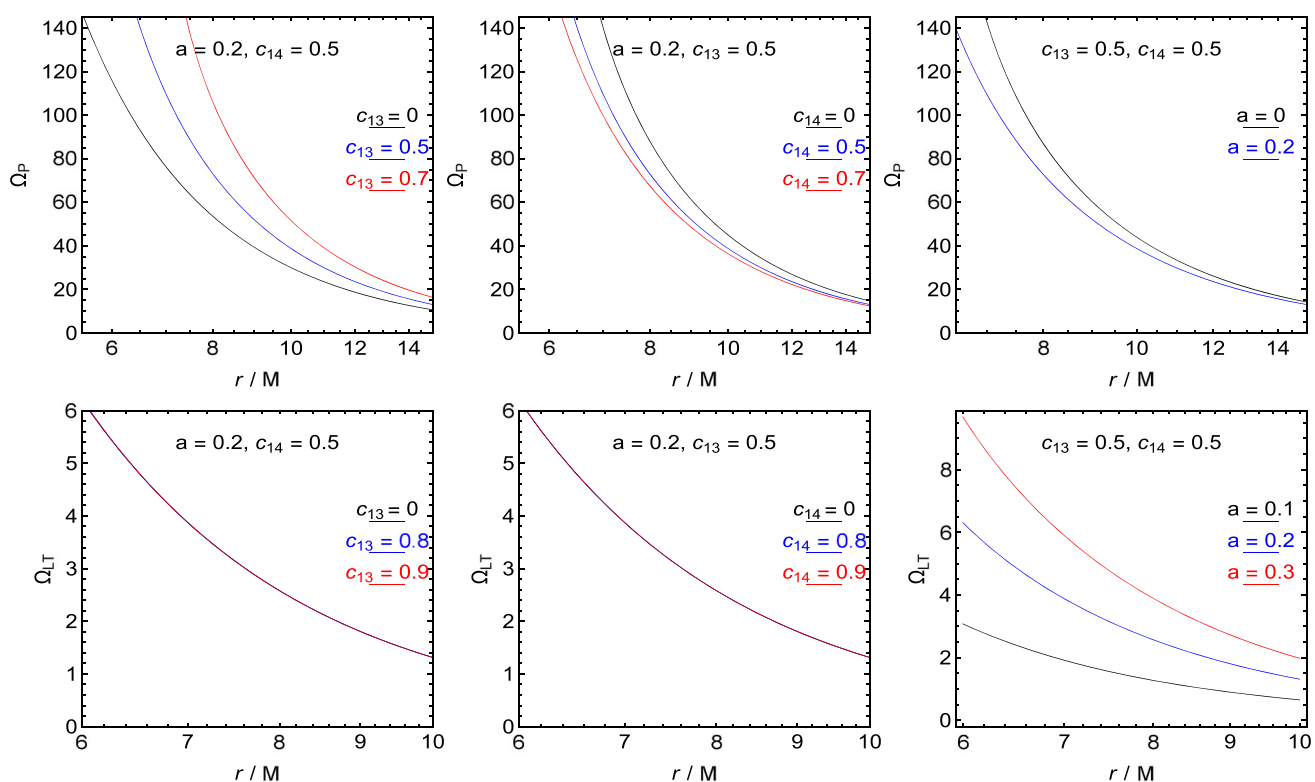


Fig. 12 Periastron and Lense–Thirring precessions for the second kind of slowly rotating E&E BH

charge Q . However, the co-rotating ISCOs shift away from the BH as the coupling parameter c_{13} is increased but move towards the BH when the rotation of BH is increased. It is noted that when the BHs rotate rapidly, smaller radii of ISCOs can be observed. The ISCOs with smaller radii can be found around the first and second kinds of slowly rotating EÆ BHs as compared to slowly rotating Kerr BH.

We have studied the fundamental frequencies of small harmonic oscillations of test particles in the radial and vertical directions related to the equatorial circular orbits and studied the radial profiles of the radial, vertical, and orbital frequencies. The orbital and vertical frequencies coincide when the rotation of BH is switched off, however, different profiles can be observed when the BH rotation is switched on. We found that the radial profiles move toward the BH when the BH rotates rapidly or charge Q or parameter c_{14} is increased. However, coupling parameter c_{13} contributes to moving the radial profiles away from the BH. The particles moving around slowly rotating Kerr BH have high frequencies as compared to moving around the first and second kinds of slowly rotating EÆ BHs.

We have explored the radial profiles of upper $\nu_U(r)$ and lower $\nu_L(r)$ frequencies for many different HF QPO models, i.e., ER model and its variants (ER0, ER1, ER2, ER3, ER4, ER5), RP model and its variant (RP1, RP2), TD and WD models and determined the position of resonance radii $r_{3:2}$. It is worth mentioning that the positions of resonant radii $r_{3:2}$ for all considered HF QPO models for the case of slowly rotating first and second kinds of EÆ BHs lie at smaller radii as compared to the slowly rotating Kerr BH. Furthermore, the resonant radius $r_{3:2}$ for the ER4 HF QPOs model is closer to the BH among all considered HF QPO models. In addition, we have also analysed the behaviour of periastron and Lense–Thirring precession frequencies for both the first and second kinds of slowly rotating EÆ BHs. Both periastron and Lense–Thirring precession frequencies can be seen high with the increase of the coupling parameters c_{13} . However, these frequencies are small when BH rotation or coupling parameter c_{14} is increased.

Acknowledgements The author SKM is thankful for continuous support and encouragement from the administration of University of Nizwa.

Data availability statement This manuscript has no associated data or the data will not be deposited. [Authors' comment: No new data were generated or analyzed in support of this research.]

Open Access This article is licensed under a Creative Commons Attribution 4.0 International License, which permits use, sharing, adaptation, distribution and reproduction in any medium or format, as long as you give appropriate credit to the original author(s) and the source, provide a link to the Creative Commons licence, and indicate if changes were made. The images or other third party material in this article are included in the article's Creative Commons licence, unless indicated otherwise in a credit line to the material. If material is not included in the article's Creative Commons licence and your intended

use is not permitted by statutory regulation or exceeds the permitted use, you will need to obtain permission directly from the copyright holder. To view a copy of this licence, visit <http://creativecommons.org/licenses/by/4.0/>.

Funded by SCOAP³. SCOAP³ supports the goals of the International Year of Basic Sciences for Sustainable Development.

References

1. A. Einstein, Sitzungsberichte der Königlich Preußischen Akademie der Wissenschaften (Berlin, 1915), p. 844
2. D. Blas, E. Lim, Int. J. Mod. Phys. D **23**, 1443009 (2014). [arXiv:1412.4828](https://arxiv.org/abs/1412.4828) [gr-qc]
3. D. Mattingly, Living Rev. Relativ. **8**, 5 (2005). [arXiv:gr-qc/0502097](https://arxiv.org/abs/gr-qc/0502097)
4. T. Jacobson, D. Mattingly, Phys. Rev. D **64**, 024028 (2001). [arXiv:gr-qc/0007031](https://arxiv.org/abs/gr-qc/0007031)
5. B. Altschul, Phys. Rev. D **72**, 085003 (2005). [arXiv:hep-th/0507258](https://arxiv.org/abs/hep-th/0507258)
6. C. Eling, T. Jacobson, D. Mattingly, arXiv e-prints. (2004). [arXiv:gr-qc/0410001](https://arxiv.org/abs/gr-qc/0410001)
7. C. Eling, T. Jacobson, Class. Quantum Gravity **23**, 5643 (2006). [arXiv:gr-qc/0604088](https://arxiv.org/abs/gr-qc/0604088)
8. R.A. Remillard, J.E. McClintock, Ann. Rev. Astron. Astrophys. **44**, 49 (2006). [arXiv:astro-ph/0606352](https://arxiv.org/abs/astro-ph/0606352)
9. Z. Stuchlík, A. Kotrlová, G. Török, Astron. Astrophys. **552**, A10 (2013). [arXiv:1305.3552](https://arxiv.org/abs/1305.3552) [astro-ph.HE]
10. Z. Stuchlík, J. Vrba, J. Cosmol. Astropart. Phys. **2021**, 059 (2021). [arXiv:2110.07411](https://arxiv.org/abs/2110.07411) [gr-qc]
11. Z. Stuchlík, J. Vrba, Astrophys. J. **935**, 91 (2022). [arXiv:2208.02612](https://arxiv.org/abs/2208.02612) [gr-qc]
12. Z. Stuchlík, J. Vrba, Eur. Phys. J. Plus **136**, 1 (2021)
13. Z. Stuchlík, J. Vrba, Universe **7**, 279 (2021)
14. C. Ding, A. Wang, X. Wang, T. Zhu, Nucl. Phys. B **913**, 694 (2016). [arXiv:1512.01900](https://arxiv.org/abs/1512.01900) [gr-qc]
15. P. Berglund, J. Bhattacharyya, D. Mattingly, Phys. Rev. D **85**, 124019 (2012). [arXiv:1202.4497](https://arxiv.org/abs/1202.4497) [hep-th]
16. R.A. Konoplya, A. Zhidenko, Phys. Lett. B **644**, 186 (2007). [arXiv:gr-qc/0605082](https://arxiv.org/abs/gr-qc/0605082)
17. R.A. Konoplya, A. Zhidenko, Phys. Lett. B **648**, 236 (2007). [arXiv:hep-th/0611226](https://arxiv.org/abs/hep-th/0611226)
18. T. Zhu, Q. Wu, M. Jamil, K. Jusufi, Phys. Rev. D **100**, 044055 (2019). [arXiv:1906.05673](https://arxiv.org/abs/1906.05673) [gr-qc]
19. M. Azreg-Aïnou, Z. Chen, B. Deng, M. Jamil, T. Zhu, Q. Wu, Y.-K. Lim, Phys. Rev. D **102**, 044028 (2020). [arXiv:2004.02602](https://arxiv.org/abs/2004.02602) [gr-qc]
20. Z. Stuchlík, M. Kolos, Mon. Not. R. Astron. Soc. **451**, 2575 (2015). [arXiv:1603.07339](https://arxiv.org/abs/1603.07339) [astro-ph.HE]
21. M. Kolos, M. Shahzadi, Z. Stuchlík, Eur. Phys. J. C **80**, 133 (2020)
22. M. Shahzadi, M. Kolos, Z. Stuchlík, Y. Habib, Eur. Phys. J. C **81**, 1067 (2021). [arXiv:2104.09640](https://arxiv.org/abs/2104.09640) [astro-ph.HE]
23. M. Kolos, Z. Stuchlík, A. Tursunov, Class. Quantum Gravity **32**, 165009 (2015). [arXiv:1506.06799](https://arxiv.org/abs/1506.06799) [gr-qc]
24. M. Kolos, M. Shahzadi, A. Tursunov, Eur. Phys. J. C **83**, 323 (2023). [arXiv:2304.13603](https://arxiv.org/abs/2304.13603) [gr-qc]
25. M. Shahzadi, M. Kolos, Z. Stuchlík, Y. Habib, Eur. Phys. J. C **82**, 407 (2022). [arXiv:2201.04442](https://arxiv.org/abs/2201.04442) [gr-qc]
26. C. Ding, A. Wang, X. Wang, Phys. Rev. D **92**, 084055 (2015). [arXiv:1507.06618](https://arxiv.org/abs/1507.06618) [gr-qc]
27. E. Barausse, T.P. Sotiriou, I. Vega, Phys. Rev. D **93**, 044044 (2016). [arXiv:1512.05894](https://arxiv.org/abs/1512.05894) [gr-qc]
28. C. Ding, Phys. Rev. D **96**, 104021 (2017). [arXiv:1707.06747](https://arxiv.org/abs/1707.06747) [gr-qc]
29. Z. Stuchlík, A. Kotrlová, Gen. Relativ. Gravit. **41**, 1305 (2009). [arXiv:0812.5066](https://arxiv.org/abs/0812.5066) [astro-ph]

30. Z. Stuchlík, J. Vrba, Eur. Phys. J. Plus **136**, 977 (2021). [arXiv:2108.09466](https://arxiv.org/abs/2108.09466) [gr-qc]
31. M.A. Abramowicz, P. Nurowski, N. Wex, Class. Quantum Gravity **12**, 1467 (1995)
32. A. Tursunov, Z. Stuchlík, M. Kolos, Phys. Rev. D **93**, 084012 (2016). [arXiv:1603.07264](https://arxiv.org/abs/1603.07264) [gr-qc]
33. S.A. Kaplan, JETP **19**, 951 (1949)
34. S. Kato, J. Fukue, S. Mineshige, Black-Hole Accretion Disks: Towards a New Paradigm, Kyoto University Press, pp 549 (2008)
35. S. Kato, Astron. Soc. Jpn. **53**, L37 (2001)
36. M. Ortega-Rodríguez, A. Silbergleit, R. Wagoner, Astrophys. Fluid Dyn. **102**, 75 (2008). [arXiv:astro-ph/0611101](https://arxiv.org/abs/astro-ph/0611101)
37. W. Klužniak, M.A. Abramowicz, arXiv e-prints (2001). [arXiv:astro-ph/0105057](https://arxiv.org/abs/astro-ph/0105057)
38. L.D. Landau, E.M. Lifshitz, The classical theory of fields, Vol. 2, fourth Edition, Butterworth-Heinemann Publisher (Elsevier) (1975)
39. Z. Stuchlík, M. Kolos, Astron. Astrophys. **586**, A130 (2016). [arXiv:1603.07366](https://arxiv.org/abs/1603.07366) [astro-ph.HE]
40. R.M. Wald, General Relativity, University of Chicago Press, Chicago (1984)
41. Z. Stuchlík, M. Kolos, J. Kovář, P. Slaný, A. Tursunov, Universe **6**, 26 (2020)
42. Z. Stuchlík, A. Kotrlová, Gen. Relativ. Gravit. **41**, 1305 (2009). [arXiv:0812.5066](https://arxiv.org/abs/0812.5066)
43. L. Stella, M. Vietri, S.M. Morsink, Astrophys. J. Lett. **524**, L63 (1999). [arXiv:astro-ph/9907346](https://arxiv.org/abs/astro-ph/9907346)
44. M. Bursa, in *RAtime 6/7: Workshops on Black Holes and Neutron Stars*, edited by S. Hledík, Z. Stuchlík (2005), pp. 39–45
45. G. Török, M.A. Abramowicz, W. Klužniak, Z. Stuchlík, Astron. Astrophys. **436**, 1 (2005)